Advances in Materials
2024, Vol. 13, No. 4, pp. 80-91
https://doi.org/10.11648/j.am.20241304.13

Research Article

Investigation Optical Properties of ZnTe@Ag Core-Shell Spherical Nanocomposites Within Varies Dielectric Host Matrices

Tsegaye Atnaf[1], **Shewa Getachew**[2, *]

[1]Department of Chemistry, Wolkite University, Addis Ababa, Ethiopia
[2]Department of Physics, Wolkite University, Addis Ababa, Ethiopia

Abstract

We theoretically and numerically investigated the local field enhancement factor (*LFEF*), absorption coefficient, refractive index, and group velocity of spherical core-shell nanocomposites (*NCs*) using the quasi-static approach. By solving Laplace's equations, we derived expressions for the enhancement factor, polarizability, absorption coefficient, refractive index, and group velocity for each core-shell *NCs*. Our findings show that the LFEF, absorption coefficient, and group velocity of spherical core-shell *NCs* exhibit two peaks, while the real part of the refractive index shows four distinct peaks. Additionally, the core-shell nanocomposites demonstrate greater tunability and a higher intensity of the enhancement factor when the host matrix is changed from *CdSe* to SiO_3. The study further reveals that, for spherical nanocomposites, the first two peaks of the enhancement factor and extinction cross-sections occur at the same frequencies. Moreover, all extinction cross-section peaks are lowest when the dielectric function of the host matrix is SiO_3, whereas the peaks are highest for *CdSe*. The variation in peak values, despite having the same number of peaks for different shapes, indicates that the shape of the core-shell *NCs* significantly influences the intensity, number, and positions of the peaks in the enhancement factor and optical cross-sections. Such nanocomposites hold potential for applications in optical sensing, biosensing, as well as in photonic and electronic devices.

Keywords

Absorption Coefficient, Host Matrix, Nanocomposites, Fast Light, Slow Light

1. Introduction

Over the past three decades, the optical properties of nanoparticles have been extensively studied using various approaches. Among them, core-shell *NCs* have shown vast applications in numerous fields of science and technology [1]. It has been observed that the optical properties of dielectric core-metallic shell *NCs* are strongly influenced by factors such as size, metal fraction, spatial distribution of the core-shell structure, and the surrounding medium [2-5]. Additional research has further demonstrated that although size and the embedding medium are important parameters, the surface plasmon resonances of core-shell nanoparticles are much more sensitive to particle shape [6]. Therefore, altering the shape of core-shell *NCs* is an effective method to tune surface plasmon resonances and, consequently, their optical

*Corresponding author: shewa.getachew@wku.edu.et (Shewa Getachew)

Received: 13 November 2024; **Accepted:** 28 November 2024; **Published:** 30 December 2024

properties. Due to their geometric shape, which allows tunability of optical properties, spheroidal core-shell *NCs* have garnered significant interest [7]. Since this geometry supports plasmon resonances, spheroidal core-shell NCs consisting of a dielectric core coated with a metallic shell are among the most useful structures for achieving a wide tunability range from the visible to the infrared regions of the electromagnetic spectrum [8, 9].

Among various combinations of core-shell nanostructures, metal@metal core-shell nanocomposites exhibit novel properties that are valuable for numerous applications. These unique characteristics Preprint submitted to primarily stem from the interaction between metallic (plasmonic) materials and the incident electro-magnetic field, significantly enhanced by the surface plasmon resonance (*SPR*) phenomenon and the interaction of metal shell plasmons with the metal interior material [10]. At the SPR frequencies, the collective oscillations of conducting electrons in the metallic nanoparticle are driven by incident resonant light, which acts as electric radiating dipoles. A two-layer bimetallic core-shell nanostructure has been investigated for desired applications both experimentally [11-14] and theoretically [15, 16]. sThe position of the surface plasmon band in core-shell nanostructures can be tuned based on size, shape, and surface morphology [17, 18]. Among these substrates, *SiO_2@Au NCs* have been completely studied in various research in chemistry and biomedicine fields over the past year due to their unique Physicochemical and plasmonic characteristics [19, 20].

At the nanoinclusion, nanoparticles (*NPs*) of both *ZnO* and Ag exhibit distinctive catalytic and optical properties, making them well-suited for medical applications. The uncoated Ag and ZnO nanoparticles have demonstrated significant antibacterial properties, leading to their widespread use in fields such as in cosmetic industry and the biomedicine [21]. In comparison to other metallic *NPs*, Ag *NPs* exhibit Ag *NPs* demonstrate reduced toxicity, outstanding biocompatibility, and antimicrobial characteristics [22-24]. *SiO_2* coated quantum dots are instrumental in biomedical applications, particularly for sensing, probing, and labeling cells and tissues due to their long-term chemical and optical stability. Furthermore, their photonic conversion capabilities make them ideal candidates for optoelectronic devices [25]. *Si_3N_4* thin films play a crucial role in modern electronic device production as diffusion masks and passivation layers. Additionally, the combination of *SiO_2* and *Si_3N_4* films has enabled the realization of a new generation of electronic devices with memory properties [26].

Moreover, since zinc telluride (*ZnTe*) can be easily doped, it finds applications in blue light emitting diodes, laser diodes, and solar cells, making it essential for optoelectronic device design. In *CdTe*/*ZnTe* solar cells, the *ZnTe* semiconductor enhances efficiency by reducing the high electron affinity of *CdTe* [27]. *ZnTe* is also utilized in nonlinear optics for producing terahertz radiation and as an electro-optical detector. Some applications of the *CdTe* semiconductor binary compound include electro-optical modulators in infrared optical materials [28, 29]. Numerous experimental, computational, and theoretical studies have explored the effect of shape on the optical properties of core-shell *NCs*, such as *SiO_2*@Au [30], Ag@*SiO_2* [31], CdSe@Ag [32], and *ZnO@Au* [33].

This paper presents computational results obtained from the study of the absorption coefficient, refractive index, and group velocity in metal-coated dielectric *NCs* with spherical nanoinclusions embedded in an active dielectric host matrix. We demonstrate that *NCs* with spherical nanoinclusions featuring dielectric cores embedded in various host matrices strongly absorb light at two resonant frequencies, unlike *NCs* with dielectric-coated metal spherical nanoinclusions, which have only one resonant frequency. The research indicates that the dielectric function (*DF*) of various host matrices substantially amplifies the intensity, absorption coefficient, refractive index, gains, and group velocity. This amplification facilitates the transmission of strongly attenuated narrow pulses of slow, backward, and fast light within the *NCs* media. The author asserts that this investigation is the first to examine the absorption coefficient, refractive index, and the occurrence of slow and fast light in NCs featuring spherical nanoinclusions, particularly those with metal-coated dielectric cores. These findings are considered original contributions to the field.

2. Theoretical Bases and Mathematical Computations

Our work focused on a type of nanocomposite material called spherical metal coated dielectric *NCs*. These *NCs* consist of a core made of a dielectric material with a radius of r_1 and a dielectric function represented by ε_d. The shell surrounding the core has a radius of r_2 and its dielectric function varies depending on the electric field applied to it, which we denote as ε_m. The entire nanocomposite is embedded within a host matrix made of a dielectric material with a dielectric function of ε_m. The nanocomposite is then exposed to incident electromagnetic radiation [8, 11]. In order to investigate the impact on the absorption coefficient, refractive index and group velocity, we explored four different dielectric function of the host matrices. Those are *CdSe*, *ZnO*, *Si_3N_4* and *SiO_3* host matrices. In this study, we separately examined both components of the *DFs* to analyze their individual effects.

2.1. Electric Potential Distribution in Spherical Metal NCs

By applying boundary conditions and solving Laplace's equation for spherical metal-coated dielectric *NCs*, the electric potential distributions within the core-shell structure and surrounding host matrix are determined. The core-shell nanocomposite consists of a dielectric core with radius r_1 and

dielectric function ε_d, and a metallic shell characterized by radius r_2 and dielectric function ε_m (where $r_1 < r_2$). The host material is described by its dielectric function, ε_h. The electric potential distributions are expressed by three distinct functions: ϕ_d for the dielectric core, ϕ_m for the metallic shell, and ϕ_h for the host matrix. These functions are derived based on the equation referenced in [12, 13].

$$\Phi_d = -E_h A r \cos\theta, r \le r_1$$

$$\Phi_m = -E_h \left(Br - \frac{C}{r^2}\right) cos\theta, r_1 \le r \le r_2$$

$$\Phi_h = -E_h \left(r - \frac{D}{r^2}\right) \cos\theta, r > r_2$$

In this scenario, E_h denotes the applied electric field, while r and θ refer to the spherical coordinates of the observation point. The z-axis is aligned with the direction of the vector E_h. The coefficients A, B, C, and D are unknowns that must be determined by applying the continuity conditions for the electric potential and displacement vector at the boundaries between the core-shell and shell-host matrix interfaces. At the boundary between the dielectric core and the metallic shell of a metal-dielectric nanocomposite, the electric potential remains continuous. This is because there cannot be a discontinuous change in the potential across the interface; thus, the potential in both the dielectric (core) and metallic (shell) regions must be equal at the interface. This condition can be expressed as:

$$\phi_d = \phi_m, r = r_1 \quad (1)$$

$$\phi_m = \phi_d, r = r_2 \quad (2)$$

The continuity of the displacement vector (which is related to the electric field) must also be maintained at the interface. This condition can be expressed as:

$$\varepsilon_d \frac{\partial \phi_d}{\partial r} = \varepsilon_m \frac{\partial \phi_m}{\partial r}, r = r_1 \quad (3)$$

$$\varepsilon_m \frac{\partial \phi_m}{\partial r} = \varepsilon_h \frac{\partial \phi_h}{\partial r}, r = r_2 \quad (4)$$

The dielectric constants of the dielectric core, metal shell, and dielectric host are represented by ε_d, ε_m, and ε_h, respectively. By solving equations 1, 2, 3 and 4 an simultaneously, the values of the unknown coefficients can be determined as listed below.

$$A = \frac{9\varepsilon_h \varepsilon_m}{2p\eta} \quad (5)$$

$$B = \frac{3\varepsilon_h(\varepsilon_d + 2\varepsilon_m)}{2p\eta} \quad (6)$$

$$C = \frac{3\varepsilon_h(\varepsilon_d - \varepsilon_m)}{2p\eta} {r_1}^3 \quad (7)$$

$$D = \left(1 - \frac{3p\varepsilon_h(\varepsilon_d - \varepsilon_m) + 9\varepsilon_h\varepsilon_m}{2p\eta}\right) {r_2}^3 \quad (8)$$

Where,

$p = 1 - \left(\frac{r_1}{r_2}\right)^3$ is the metal volume fraction in the inclusion,

$$\eta = {\varepsilon_m}^2 + \prod \varepsilon_m + \varepsilon_d \varepsilon_h \quad (9)$$

$$\prod = \left(\frac{3}{2p} - 1\right)\varepsilon_d + \left(\frac{3}{p} - 1\right)\varepsilon_h \quad (10)$$

The Drude-Sommerfeld model is a theoretical framework that describes the behavior of electrons in metals, offering a simplified yet effective method for understanding their electrical and optical properties. This model yields a straightforward expression for the metal's dielectric function (ε_m), which indicates how the material responds to an external electric field and influences its optical characteristics. According to the Drude-Sommerfeld model, the *DF* of the metal (ε_m) is expressed as follows [8, 9]:

$$\varepsilon_m = \varepsilon_\infty - \frac{1}{z(z + i\gamma)} \quad (11)$$

In this context, ε_∞ denotes the effect of bound electrons on polarizability. The variable z represents the ratio of the incident radiation frequency (ω) to the frequency of the bulk plasmon (ω_p), while γ indicates the ratio of the electron damping constant (ν) to the plasma frequency (ω_p). Additionally, the real and imaginary components of ε_m can be expressed as

$$\varepsilon_m = \varepsilon'_m + i\varepsilon''_m \quad (12)$$

Let's denote the parts, both real and imaginary of the equations above as follows:

$$\varepsilon'_m = \varepsilon'_\infty - \frac{1}{z(z+\gamma)}$$

$$\varepsilon''_m = \varepsilon''_\infty + \frac{1}{z(z^2+\gamma z)}$$

2.2. Dispersion Properties of Metal-Dielectric Composites with Spherical Nanoinclusions

Dispersion is the phenomenon in which the refractive index or other optical properties of a material change with the frequency or wavelength of light. In the case of composites containing spherical nanoinclusions, dispersion occurs due to the interaction between the nanoinclusions and the sur-rounding matrix material. The incorporation of spherical nanoinclusions within a nanocomposite (*NCs*) creates additional interfaces, leading to complex interactions with incident electromagnetic waves. These interactions can result in dispersion phenomena, such as a frequency-dependent refractive index, absorption, and scattering. The polarization of an individual metal covered

spherical nanoinclusion with a dielectric core embedded in a dielectric host matrix can be presented as follows [2, 14, 15]:

$$D = \alpha r_2^2 = \alpha = 1 - \frac{3}{2}\frac{\Delta}{\eta} \quad (13)$$

Where,

$$\Delta = \varepsilon_h\left(\left(\frac{3}{2p} - 1\right)\varepsilon_m + \varepsilon_d\right)$$

Here, D represents the effective polarizability of the inclusion, while p denotes the metal fraction of the inclusion (r_1 and r_2 are the radii of the dielectric core and the metal shell, respectively). Since ε_m is complex, the terms $\Delta, \alpha, \prod$ and η are also complex.

2.3. Refractive Index of Composite with Passive Host Matrix

The effective dielectric function (ε_e) of the composite can be determined using the Clausius Mossotti formula [15]

$$\frac{\varepsilon_e - \varepsilon_h}{\varepsilon_e + 2\varepsilon_h} = \frac{4\pi}{3} DN \quad (14)$$

Where D is defined by equation (13), and N represents the density of the inclusions. The effective dielectric function, ε_e, is provided by the equation below.

$$\varepsilon_e = \varepsilon_h\left(1 + 3f\frac{\alpha}{1 - f\alpha}\right) = n^2 \quad (15)$$

Where, $f = \frac{4\pi}{3} r_2^3 N$ represents the volume fraction of spherical inclusions, and α denotes the polarizability of the inclusions.

$$n^2 = \varepsilon_h\left(1 + 3f\frac{\alpha' + i\alpha''}{1 - f(\alpha' + i\alpha'')}\right)$$

$$n^2 = \varepsilon_h\left(1 + 3f\frac{\alpha' - f|\alpha|^2 + i\alpha''}{(1 - f\alpha')^2 + (f\alpha'')^2)}\right) = b_1 + ib_2 \quad (16)$$

Where,

$$b_1 = \varepsilon_h\left(1 + 3f\frac{\alpha' - f|\alpha|^2 + i\alpha''}{(1 - f\alpha')^2 + (f\alpha'')^2)}\right)$$

$$b_2 = \varepsilon_h\, 3f\frac{\alpha''}{(1 - f\alpha')^2 + (f\alpha'')^2)}$$

Equating the real and the imaginary parts $n = n' + in''$ with equation (16) can give us the expressions

$$n'^2 - n''^2 = b_1 \quad (17)$$

$$2n'n'' = b_2 \quad (18)$$

In this representation, the refractive index is divided into its real part, denoted as n', and its imaginary part, denoted as n''. By isolating these real and imaginary components, we can effectively express the refractive index in terms of b_1 and b_2.

$$n'^2 = \frac{1}{2}\left(\sqrt{b_1^2 + b_2^2} + b_1\right) \quad (19)$$

$$n''^2 = \frac{1}{2}\left(\sqrt{b_1^2 + b_2^2} + b_1\right) \quad (20)$$

These equations are utilized to numerically compute the n' and n'' of composites that contain metal coated dielectric inclusions for various host matrices.

2.4. Absorption Coefficient

The wave equation allows for a solution represented as a plane wave given by $E=E_0 e^{i(k'x-\omega t)}$. The wave number $k = n\omega/c$ is a complex quantity that can be expressed in the form $k = k' + ik''$. Therefore, we can rewrite the equation above as [34]:

$$E = E_0 e^{i(k'x-\omega t)} e^{-ik''x} \quad (21)$$

The term $e^{-ik''x}$ indicates that the wave diminishes as it travels. The intensity of an electromagnetic wave is proportional to the square of the electric field (i.e., $I \approx E^2$). According to Beers law, we can express the relationship as follows:

$$I = I_0 e^{-\alpha''_{abs}x} \quad (22)$$

where α_{abs} is known as the absorption coefficient. Therefore, we can write the absorption coefficient as

$$\alpha_{abs} = 2k'' = 2n''\omega/c \quad (23)$$

$$\alpha_{abs} = 2n''z\omega_p/c \quad (24)$$

2.5. Group Velocity

The group velocity v_g of a wave packet is the velocity at which the overall shape of the wave packet (or pulse) travels. This is particularly important when dealing with wave packets composed of multiple waves with different wave numbers k. If the angular frequency $\omega(k)$ is a linear function of k, the wave packet will move without distortion, maintaining its shape. This is because all components of the wave packet travel at the same speed. The group velocity v_g is defined as the derivative of the angular frequency $\omega(k)$ with respect to the wave number k. In the case where the angular frequency $\omega(k)$ is approximately linear near the central wave number k_0, the group velocity v_g around that point k_0 is given by:

$$v_g = \frac{d\omega}{dk} \quad (25)$$

This expression shows that the velocity at which the pulse travels is determined by the slope of the ω(k) versus k curve at the central wave number k_0. When the wave packet moves with this velocity, it remains undistorted, as all components of the wave packet move together coherently. The group velocity v_g of a wave packet can be expressed in terms of the group refractive index n_g as follows:

$$v_g = \frac{c}{n_g} \tag{26}$$

Where, c is the speed of light in a vacuum. The group refractive index n_g is related to the ordinary refractive index $n(z)$ by:

$$n_g = n(z) + \omega \frac{dn(z)}{dz} \tag{27}$$

This expression reflects that different frequency components of a wave packet propagate at varying speeds due to dispersion, which ultimately affects the overall group velocity of the wave packet. Slow light occurs when the group velocity v g of light is significantly less than the speed of light in a vacuum c. The condition $\frac{dn}{d\omega} \ll c$ signifies that the dispersion is such that the group velocity is considerably diminished. In the context of normal dispersion ($\frac{d\omega}{dk} > 0$), where the refractive index n exceeds 1, the group velocity is lower than the phase velocity. This occurs because the refractive index n increases with frequency, resulting in a reduction in group velocity. Conversely, fast light pertains to scenarios where the group velocity v_g surpasses the speed of light in a vacuum c or even turns negative. This phenomenon is typically linked to anomalous dispersion. In regions characterized by anomalous dispersion, where $\frac{d\omega}{dk} < 0$ (indicating that the refractive index decreases with frequency), the group velocity can indeed become negative. However, this does not mean that information or energy travels faster than c; rather, it suggests that the peak of the pulse appears to move in the opposite direction to the wave vector.

3. Results and Discussion

In this study, we examined the enhancement factor, absorption coefficients, refractive index, and group velocity of ZnTe@Ag core-shell spherical nanoparticles embedded in various host matrices. The model taken into account in this study specifically includes a dielectric core of ZnTe, a silver (Ag) shell, and different host materials. The parameters selected for numerical calculations are as follows [35, 36]: $\varepsilon_d = 9.8$, $\varepsilon_\infty = 4.5$, $\omega_p = 1.45\ x\ 10^{14} rad/s$, $\upsilon = 1.67\ x\ 10^{14} rad/s$, and z = 0.2.

3.1. Effect of Core-Shell Radii on *LFEF* of Metal Coated Dielectric Spherical *NCs*

Figure 1 illustrates the plot of the *LFEF* for five different core-shell radii, while maintaining a constant shell thickness (r_2) of 40nm. The analysis indicates that the *LFEF* of the spheroidal core-shell *NCs* displays two distinct peaks. As the core-shell radii increase from 0.4 to 0.6, the first resonance peak (counted from left to right) of the *LFEF* for the spherical core-shell *NCs* moves toward lower frequencies, whereas the second peak of resonance (counted from right to left) shifts toward higher frequencies. This behavior can be understood through the plasmon hybridization theory within the quasi-static limit [37, 38]. In this theory, sphere and cavity plasmons are generated on the outer and inner surfaces of the nanoshell, respectively., and these plasmons hybridize to produce two new resonance modes: the lower energy plasmon mode is symmetric, while the higher energy plasmon mode is antisymmetric [39]. The intensity of these plasmon modes is influenced by the metallic shell's thickness. The asymmetric and antisymmetric plasmonic modes are represented by the first and second peaks of resonance peaks, respectively. The first set of peaks increases in value and experiences a blue shift as the metallic shell's thickness increases (i.e., as r_1/r_2 decreases). This enhancement is attributed to a rise in the number of available free electrons that participate in the surface plasmon oscillations at the Ag/ZnO interface [40].

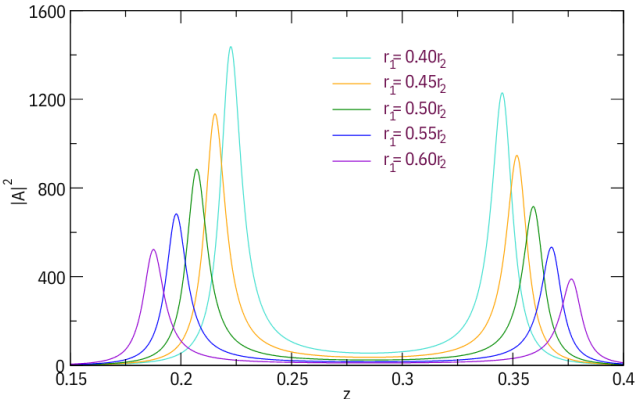

Figure 1. *LFEF ($|A|^2$) as a function of frequency for different core-shell radii. r_2 = 0.40nm fixed constant.*

When the magnitude of the NPs is increased (i.e., the magnitude of the ZnTe@Ag core-shell, while keeping the shell thickness constant) from r_1/r_2 = 0.4 to r_1/r_2 = 0.6, the values of the two resonance peak sets are are enhanced, although the peak positions remain unchanged. This indicates that the magnitude of the NCs does not influence the locations of the resonant peaks; rather, it is the shift in the ratio r_1/r_2 that is the role of adjusting the peak locations to the intended wavelength, supposing that all other variables stay constant. Figures 1 and

2 emphasizes the significance of both the core-shell radii and the size of the nanoparticles in determining the optical properties of spheroidal core-shell NCs, especially in tuning and enhancing the resonance peaks of the LFEF. The findings presented in [13] are consistent with these findings.

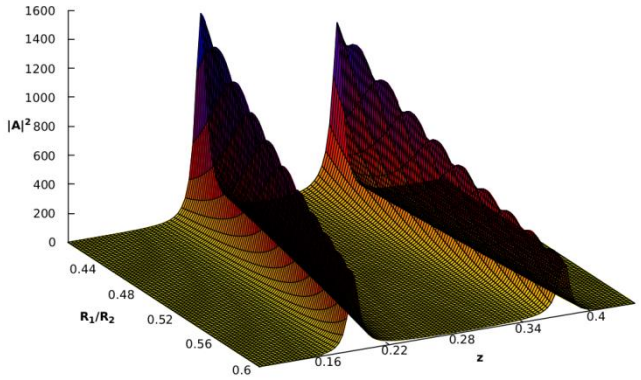

Figure 2. *LFEF for spherical nanoparticles versus core-shell radii (R_1/R_2) and frequency z in linear host matrix.*

The ability to adjust the resonance peaks of the LFEF by modifying the core-shell ratio offers a powerful tool for engineering the optical and plasmonic properties of spheroidal core-shell NCs, with important implications for various applications in photonics, optoelectronics, sensing, and nanoscale energy technology. Figure 2 presents a 3D view of figure 1.

3.2. Effect of Metal Volume Fractions on Refractive Index of Metal Coated Dielectric Spherical *NCs*

The study reveals that the number of maximum peaks in the absorption cross-section for nanocomposites varies based on the host matrix. In particular, it was observed that spherical nanocomposites exhibit two distinct peaks.

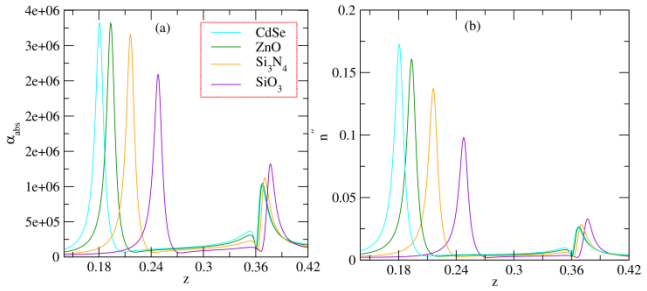

Figure 3. *(a) Absorption cross section (α_{abs}) and (b) refractive index as a function of frequency for different host matrix, r_2 = 0.40nm fixed constant.*

Using equation (24), figure 3 illustrates that the imaginary part of the refractive index and the absorption coefficient are directly proportional to each other. The typical light propagation length in the medium can be determined using the formula $l \approx 1/\alpha_{abs}$ [41]. To create conditions that allow for significant light wave propagation, it is essential to change the dielectric within the host matrix from *CdSe* to SiO_3. It is possible to succeed by introducing various dielectric functions for the host matrix. The host matrix containing SiO_3 enhances the incident electromagnetic wave instead of absorbing it.

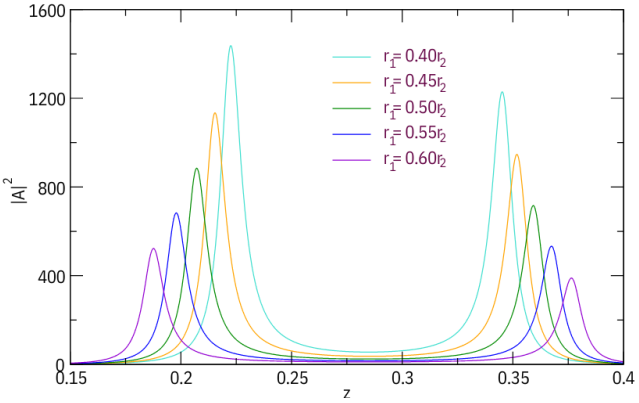

Figure 4. *(a) Real of refractive index (α_{abs}) and (b) imaginary of refractive index for different core-shell radii.*

Additionally, the study demonstrates that even when the amount of peaks remains consistent across various host matrices, their magnitudes can vary. This indicates that the host matrix of core-shell *NCs* influences both the number and the relative intensities of the absorption cross-section peaks. Figure 3(a) also shows that the resonance position of the first peak experiences a slight red shift when the host matrix of the spherical *NCs* transitions from *CdSe* to SiO_3. Conversely, a blue shift is observed when the host matrix has been modified in the opposite direction.

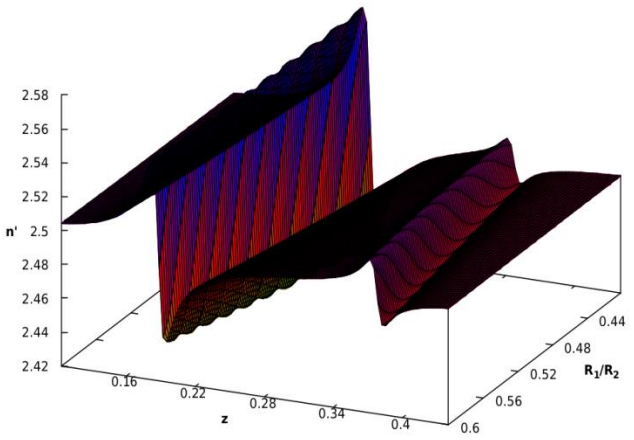

Figure 5. *Real refractive index versus resonate dimensionless frequency (z) and core-shell radii r_1/r_2 in SiO_3 host matrix.*

These shifts result in the first and second peaks becoming closer together in the SiO_3 host matrix compared to the other dielectric constants investigated. The study emphasizes the substantial the host matrix influence on the number, magnitudes, and resonance positions of the absorption cross-section peaks in spherical *NCs*. These findings offer valuable insights for a deeper understanding and optimization of the optical properties of these nanostructures. Figure 3(b) shows that there are two maximum peaks in the refractive index, which occur at different frequencies and volume fractions. When the dielectric host matrix of the spherical *NCs* changes from *CdSe* to SiO_3, the amount of the first peak decreases, while the second peak experiences a slight increase. Furthermore, both the first and second resonance peaks of the refractive index shift toward higher frequencies. Importantly, the shift of the first maximum peak toward higher frequencies is more pronounced than that of the second maximum peak. This observation indicates that the varying host matrix of the spherical *NCs* influences the first and second resonance peaks of the refractive index.

In Figure 4(a), n' is plotted against z, while Figure 4(b) presents n'' versus z. These figures focus on the resonant frequencies of a composite material composed of metal-coated dielectric spherical inclusions within a passive dielectric core, with different metal fractions indicated by p. The results reveal two peak values for both n' and n'' at distinct resonant frequencies.

Notably, the peak on the left side of the graph is of greater magnitude than the peak on the right, as shown in both n' and n''. This difference indicates an asymmetry in the refractive index properties of the composite material. Similarly, Figure 4(a) and (b), as well as Figures 5 and 6, illustrate the impact of core-shell radii on the real and imaginary parts of the refractive index of the composite material. As the ratio of the core radius to the shell radius (r_1/r_2) decreases, the first resonance peak increases (blue shift), while the second maximum peak slightly decreases (red shift). The relationship between the absorption coefficient (α_{abs}) and the refractive index (n'') is illustrated in Figure 7(a) and (b), as outlined in equation (24).

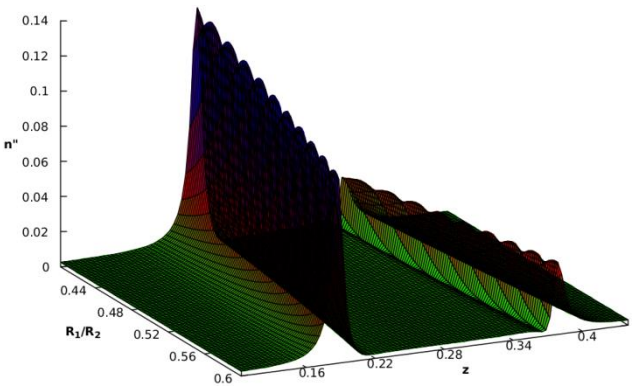

Figure 6. *Refractive index imaginary part (n'') versus resonate dimensionless frequency (z) and core-shell radii r_1/r_2 in SiO_3 host matrix.*

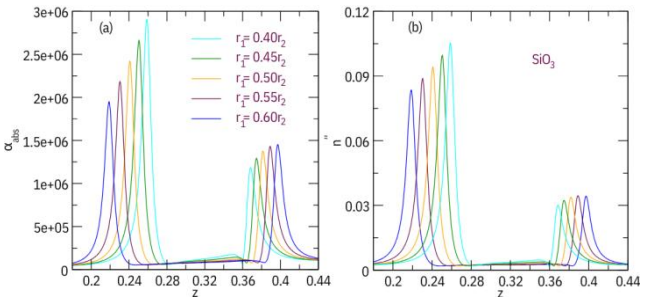

Figure 7. *(a) Absorption cross section (α_{abs}) and (b) refractive index as a function of frequency for different core-shell radii in SiO_3 host matrix.*

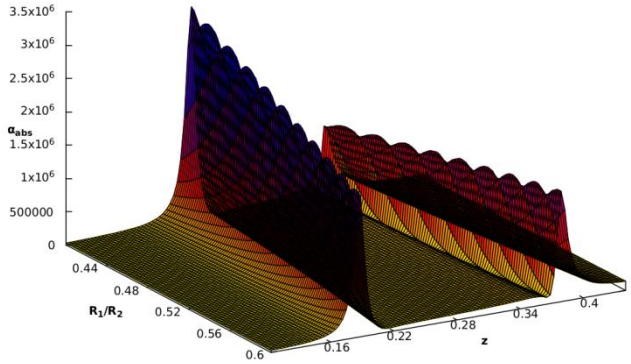

Figure 8. *Absorption coefficient (α_{abs}) versus resonate dimensionless frequency (z) and core-shell radii r_1/r_2 in SiO_3 host matrix.*

The figure displays the absorption coefficients and refractive index as functions of frequency for various core-shell ratios of the spherical nanoparticles. The absorption of the effective medium composite reaches a maximum at two distinct frequencies. As the core-shell radii of the spherical nanoparticles decrease, the first resonance peak not only increases but also shifts toward higher frequencies (a blue shift). This indicates that the composite material demonstrates stronger absorption at the first resonance frequency as the core-shell ratio decreases. The second resonate peak shows a slight decrease and shifts towards lower frequencies (red shift). This indicates that the absorption at the second resonance frequency decreases marginally as the core-shell ratio declines.

These findings illustrate the essential role of the SiO_3 host matrices in modulating the absorption coefficients and refractive index of the effective composite material. The study emphasizes the considerable impact of the core-shell structure on the resonance peaks and optical properties of the *NCs* material that includes spherical nanoparticles. Similarly, Figure 8 depicts the effect of core-shell radii on the absorption coefficients of the composite material. As the ratio of the core radius to the shell radius (r_1/r_2) decreases, the first resonance peak increases (blue shift), while the second maximum peak experiences a slight decrease (red shift). The study also performed numerical calculations and plotted the absorption coefficient of the composite material, taking into account

various volume fractions (f) of spherical nanoparticles, as illustrated in Figure 9.

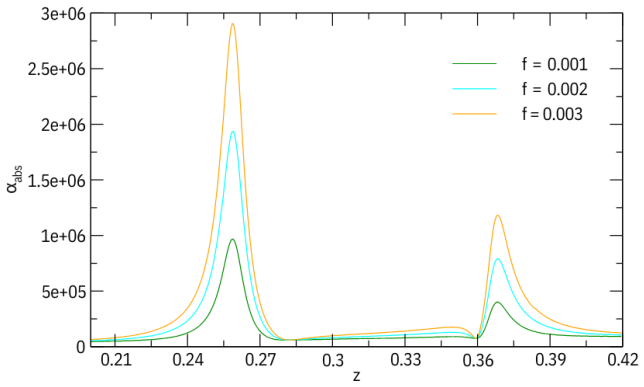

Figure 9. *Absorption cross section (α_{abs}) as a function of frequency for different volume fraction in SiO_3 host matrix and r_2 = 0.40nm fixed constant.*

The results indicate the existence of two maxima in the absorption coefficient, which occur at two distinct frequencies and volume fractions. As the volume fraction of the spherical nanoparticles rises from 0.001 to 0.003, the magnitude of the first peak increases, while the second peak exhibits a slight rise. Additionally, neither the first nor the second resonance peaks of the absorption coefficient shift; instead, they increase at two constant frequencies. This finding implies that the first and second resonance peaks of the absorption coefficient are influenced by the changing volume fraction of the spherical nanoparticles.

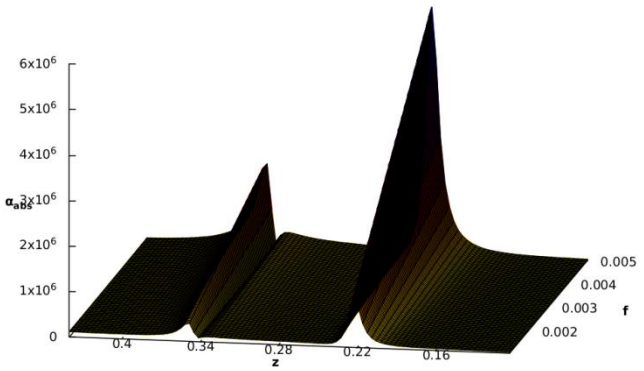

Figure 10. *Absorption cross section (α_{abs}) versus frequency and volume fraction in SiO_3 host matrix and r_2=0.40nm fixed constant.*

The investigation of the absorption coefficient (α_{abs}) is currently being conducted in both *2D* and *3D* formats. While the primary focus is on the *2D* analysis, Figure 10 illustrates the absorption coefficient in a *3D* context. Interestingly, the physical quantities depicted in Figures 9 and 10 are the same, despite the differences in dimensionality. However, there are significant distinctions between the *2D* and *3D* graphs regarding the volume fraction of spherical nanoparticles (*NPs*) within the composite material. Figure 10 demonstrates a clear relationship between the dimensionless frequency, the volume fraction of the composite, and the absorption coefficient (α_{abs}) of the spherical nanocomposites. Specifically, as the volume fraction of the composite decreases, the α_{abs} also declines accordingly. This observed trend has important implications for the light propagation properties of the nanocomposite material. The results suggest that as the α_{abs} of the nanocomposites decreases, the typical light propagation length within the medium increases, as described by the inverse relationship l= 1/α_{abs}.

Consequently, the main observation is that as the volume fraction of the composite material decreases, the absorption coefficient also decreases, resulting in an increased light propagation length within the nanocomposites. The ability to adjust the light propagation length in these nanocomposites facilitates the optimization of light-matter interactions, which is essential for developing efficient and versatile photonic and optoelectronic devices. Controlling light propagation can enhance light harvesting, trapping, guiding, and manipulation, ultimately leading to improved performance across various applications.

3.3. Effect of Varying Host Matrix on Group Velocity

Figures 11 and 12 present the group index and group velocity for spherical nanoparticles (*NPs*) in different host matrices, specifically SiO_3 and Si_3N_4, respectively. The numerical results presented in Figure 11(b) demonstrate that the group velocity of light within the SiO_3 host matrix displays two distinct behaviors. In the proximity of the first resonant frequency, the group velocity corresponds to that of "fast light", with a value of v_g=*1.86c*. Conversely, in the region of the second resonant frequency, the group velocity reflects that of "slow light", with a value of v_g=*0.96c*. Altering the dielectric host matrix of the spherical *NPs* significantly influences the results.

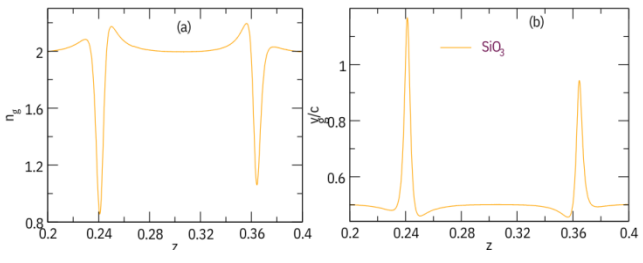

Figure 11. *Group index (n_g) and group velocity (v_g/c) in SiO_3 host matrix and r_2=0.40nm fixed constant.*

The plots of the normalized group velocity (v_g/c) against the parameter z in Figure 11(b) and Figure 12(b) for the SiO_3 and Si_3N_4 host matrices, respectively, exhibit similar

types of curves. In the SiO_3 host matrix, the first peak on the left displays fast-light group velocities, with $v_g = 1.86c$, while the second peak on the right shows slow-light group velocities, with $v_g = 0.95c$, as illustrated in figure 11. For the Si_2N_4 host matrix in figure 11, both the first peak on the left and the second peak on the right exhibit slow-light group velocities. The first peak has a group velocity of $v_g = 0.94c$, while the second peak has a group velocity of $v_g = 0.58c$. These results indicate that the dielectric host matrix of the spherical *NCs* is critical in determining the group velocities of light, resulting in the observed fast-light and slow-light phenomena.

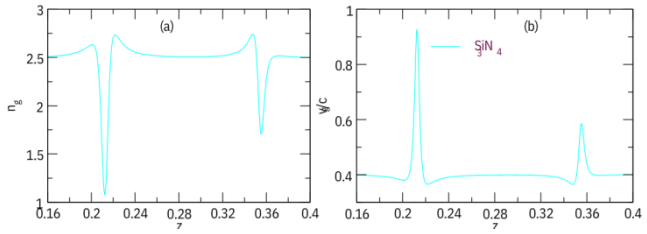

Figure 12. *Group index (n_g) and group velocity (v_g/c) in Si_3N_4 host matrix and r_2 =0.40nm fixed constant.*

This study emphasizes the importance of the host matrices in influencing the optical properties of the nanocomposite material containing spherical nanoparticles.

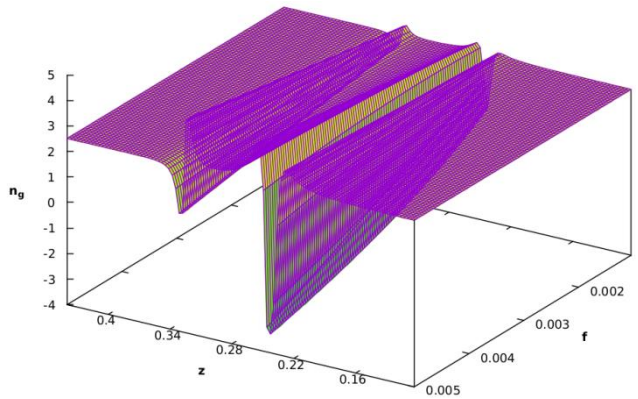

Figure 13. *Group index (n_g) versus dimensionless frequency (z) and volume fraction (f) in SiO_3 host matrix and r_2=0.40nm fixed constant.*

Figure 13 illustrates the relationship among the group index, dimensionless frequency, and volume fraction. The results indicate that as the volume fraction increases, the group index decreases into the negative range while remaining constant in the positive range. The resonant frequencies of the nanoparticles are significantly influenced by the dielectric environment of the host matrices. In the SiO_3 matrix, the first and second resonant frequencies correspond to fast light and slow light behaviors, respectively. Conversely, in the Si_2N_4 matrix, both the first and second resonant frequencies display slow light behavior. The differences in dielectric properties, resonant frequencies, light-matter interactions, and dispersion characteristics between the SiO_3 and Si_2N_4 host matrices are key factors affecting the observed variations in group velocity, particularly the contrast between fast light and slow light behaviors.

4. Conclusions

In this study, we explored the optical properties of core-shell spherical nanoinclusions embedded in various host matrices. We conducted both theoretical and numerical analyses of the *LFEF*, absorption coefficient, refractive index, and group velocity of the system using the quasistatic approximation. Our findings indicate that there are two maximum values of the local field enhancement factor for different core-shell radii and host matrices. Consequently, the behavior of local field enhancement is significantly influenced by the core-shell radii and the host matrix. As the core-shell radii increase from 0.4 to 0.6, the first resonance peak (counted from left to right) of the *LFEF* for the spherical core-shell nanocomposites shifts towards lower frequencies, while the second resonance peak (counted from right to left) shifts towards higher frequencies. Furthermore, our study shows that both the first and second resonate peaks of the refractive index shift towards higher frequencies, with the first peak demonstrating a more significant shift compared to the second. This observation suggests that the varying host matrix of the spherical nanocomposites plays a crucial role in controlling the first and second resonance peaks of the refractive index.

The effective medium composite absorption reaches a maximum at two distinct frequencies. As the core-shell radii of the spherical nanoparticles decrease, the first resonance peak increases and shifts towards higher frequencies (a blue shift), indicating that the composite material exhibits stronger absorption at the first resonance frequency as the core-shell ratio decreases. Conversely, the second resonate peak slightly decreases and shifts towards lower frequencies (a red shift), suggesting that absorption at the second resonance frequency is slightly lower as the core-shell ratio decreases. These results demonstrate that the SiO_3 host matrices significantly influence the absorption coefficients and refractive index of the effective composite material. The interaction between the incident light and the nanoparticles is affected by the dielectric properties of the host matrix. In the SiO_3 matrix, the light-matter interaction is stronger, leading to more pronounced fast light and slow light effects. In contrast, the light-matter interaction in the Si_2N_4 matrix is less pronounced, resulting in a more uniform slow light behavior. The differences in dielectric properties, resonant frequencies, light-matter interaction, and dispersion characteristics between the SiO_3 and Si_2N_4 host matrices are key factors influencing the observed differences in group velocity, particular-

ly regarding the contrast between fast light and slow light behaviors. We hope that the results obtained will have potential applications in optoelectronic and photonic devices based on *ZnTe@Ag* spherical nanocomposites.

Abbreviations

LFEF	Local Field Enhancement Factor
NCs	Nanocomposites
NPs	Nanoparticles
ZnTe	Zinc Telluride
DFs	Dielectric Functions
SPR	Surface Plasmon Resonance
SERS	Surface Enhanced Raman Spectroscopy

Author Contributions

Shewa Getachew: Conceptualization, Formal analysis, Investigation, Methodology, Software, Supervision, Visualization, Writing - original draft, Writing - review & editing

Tsegaye Atnaf: Conceptualization, Formal analysis, Methodology, Investigation, Supervision, Validation, Writing - review & editing

Data Availability Statement

This manuscript has no associated data or the data will not be deposited.

Conflicts of Interest

The authors declare no conflicts of interest.

References

[1] Bennink, R. S., Yoon, Y. K., Boyd, R. W., & Sipe, J. E. Accessing the optical nonlinearity of metals with metal-dielectric photonic bandgap structures. *Optics Letters*. 1999, *24*(20), 1416-1418.

[2] Arnold, S., O'Keeffe, T. R., Leung, K. M., Folan, L. M., Scalese, T., & Pluchino, A. Optical bistability of an aqueous aerosol particle detected through light scattering: theory and experiment. *Applied optics*. 1990, *29*(24), 3473-3478. https://doi.org/10.1364/AO.29.003473

[3] Mahmudin, L., Suharyadi, E., Utomo, A. B. S., & Abraha, K. Optical properties of silver nanoparticles for surface plasmon resonance (SPR)-based biosensor applications. *Journal of Modern Physics. 2015*, *6*(08), 1071. http://dx.doi.org/10.4236/jmp.2015.68111

[4] Pustovalov, V. K. (2023). Optical properties of nanoparticles dispersed in ambient medium and their dependences on temperature. Current Nanomaterials, 8(3), 233-258. http://dx.doi.org/10.2174/2405461508666221102090945

[5] Brandl, D. W., & Nordlander, P. (2007). Plasmon modes of curvilinear metallic core/shell particles. The Journal of chemical physics, 126(14). https://doi.org/10.1063/1.2717167

[6] Lisiecki I, Billoudet F and Pileni M. Copper Nanoparticles for Printed Electronics: Routes Towards Achieving Oxidation Stability, The Journal of Physical Chemistry, 1996, 100 41606. https://doi.org/10.3390/ma3094626

[7] Lv, W., Phelan, P. E., Swaminathan, R., Otanicar, T. P., & Taylor, R. A. (2013). Multifunctional core-shell nanoparticle suspensions for efficient absorption. *Journal of solar energy engineering*, *135*(2), 021004. https://doi.org/10.1115/1.4007845

[8] Daneshfar, N., & Noormohamadi, Z. (2020). Optical surface second harmonic generation from plasmonic graphene-coated nanoshells: influence of shape, size, dielectric core and embedding medium. *Applied Physics A*, *126*(1), 55. https://doi.org/10.1007/s00339-019-3228-y

[9] Cui, W., Li, M., Dai, Z., Meng, Q., & Zhu, Y. (2014). Near-field optical effect of a core-shell nanostructure in proximity to a flat surface. *The Journal of Chemical Physics*, *140*(4). https://doi.org/10.1063/1.4862800

[10] Encina, E. R., Pérez, M. A., & Coronado, E. A. (2013). Synthesis of Ag@ ZnO core–shell hybrid nanostructures: an optical approach to reveal the growth mechanism. *Journal of nanoparticle research*, *15*, 1-12. http://dx.doi.org/10.1007/s11051-013-1688-0

[11] Boote, B. W., Byun, H., & Kim, J. H. (2013). One-pot synthesis of various Ag–Au bimetallic nanoparticles with tunable absorption properties at room temperature. *Gold Bulletin*, *46*, 185-193. https://doi.org/10.1007/s13404-013-0099-4

[12] Shao, H., Ma, Q., Dong, X., Yu, W., Yang, M., Yang, Y.,... & Liu, G. (2015). Electrospun flexible coaxial nanoribbons endowed with tuned and simultaneous fluorescent color-electricity-magnetism trifunctionality. *Scientific Reports*, *5*(1), 14052.

[13] Hirpha, T. T., Bergaga, G. D., Ali, B. M., & Gebre, S. S. (2023). Local field enhancement factor of spheroidal core–shell nanocomposites with *passive and* active dielectric cores. *Materials Research Express*, *10*(4), 045005.

[14] Srnová-Šloufová, I., Lednický, F., Gemperle, A., & Gemperlová, J. (2000). Core− shell (Ag) Au bimetallic nanoparticles: analysis of transmission electron microscopy images. *Langmuir*, *16*(25), 9928-9935.

[15] Naseri, T., & Pour-Khavari, F. (2020). Bimetallic core-shell with graphene coating nanoparticles: enhanced optical properties and slow light propagation. *Plasmonics*, *15*(4), 907-914. https://doi.org/10.1007/s11468-019-01101-w

[16] Chahinez, D., Reji, T., & Andreas, R. (2018). Modeling of the surface plasmon resonance tunability of silver/gold core–shell nanostructures. RSC advances, 8(35), 19616-19626. https://doi.org/10.1039/c8ra03261k.

[17] Shabaninezhad, M., & Ramakrishna, G. (2019). Theoretical investigation of size, shape, and aspect ratio effect on the

LSPR sensitivity of hollow-gold nanoshells. *The Journal of chemical physics*, *150*(14). https://doi.org/10.1063/1.5090885

[18] Jackson, J. B., Westcott, S. L., Hirsch, L. R., West, J. L., & Halas, N. J. (2003). Controlling the surface enhanced Raman effect via the nanoshell geometry. *Applied Physics Letters*, *82*(2), 257-259. https://doi.org/10.1063/1.1534916

[19] Madamsetty, V. S., Mukherjee, A., & Mukherjee, S. (2019). Recent trends of the bio-inspired nanoparticles in cancer theranostics. *Frontiers in pharmacology*, *10*, 1264. https://doi.org/10.3389/fphar.2019.01264

[20] Cholkar, K., Hirani, N. D., & Natarajan, C. (2017). Nanotechnology-based medical and biomedical imaging for diagnostics. In *Emerging nanotechnologies for diagnostics, drug delivery and medical devices* (pp. 355-374). Elsevier.

[21] Yuwen, L., Sun, Y., Tan, G., Xiu, W., Zhang, Y., Weng, L.,... & Wang, L. (2018). MoS 2@ polydopamine-Ag nanosheets with enhanced antibacterial activity for effective treatment of Staphylococcus aureus biofilms and wound infection. Nanoscale, 10(35), 16711-16720. https://doi.org/10.1039/c8nr04111c

[22] Crisan, C. M., Mocan, T., Manolea, M., Lasca, L. I., Tăbăran, F. A., & Mocan, L. (2021). Review on silver nanoparticles as a novel class of antibacterial solutions. *Applied Sciences*, *11*(3), 1120. https://doi.org/10.3390/app11031120

[23] Jabeen, S., Qureshi, R., Munazir, M., Maqsood, M., Munir, M., Shah, S. S. H., & Rahim, B. Z. (2021). Application of green synthesized silver nanoparticles in cancer treatment—a critical review. *Materials Research Express*, *8*(9), 092001.

[24] Muruganandham, M., Al-Otibi, F. O., Alharbi, R. I., Sivasubramanian, K., Chaulagain, A., Velmurugan, P., & Basavegowda, N. (2023). Tabebuia rosea seed extract mediated synthesis of silver nanoparticles with antibacterial, antioxidant, and antiproliferative activities. *Materials Research Express*, *10*(12), 125006. https://doi.org/10.1088/2053-1591/ad1357

[25] Wang, N., Koh, S., Jeong, B. G., Lee, D., Kim, W. D., Park, K.,... & Lee, D. C. (2017). Highly luminescent silica-coated CdS/CdSe/CdS nanoparticles with strong chemical robustness and excellent thermal stability. *Nanotechnology*, *28*(18), 185603. https://doi.org/10.1088/1361-6528/aa6828

[26] Bauer, J. (1977). Optical properties, band gap, and surface roughness of Si3N4. *physica status solidi (a)*, *39*(2), 411-418. https://doi.org/10.1002/pssa.2210390205

[27] Suthar, D., Chuhadiya, S., Sharma, R., & Dhaka, M. S. (2022). An overview on the role of ZnTe as an efficient interface in CdTe thin film solar cells: a review. *Materials Advances*, *3*(22), 8081-8107. https://doi.org/10.1039/D2MA00817C

[28] Biswas, A., Bhardwaj, S., Boruah, T., & Dey, R. S. (2022). Electrochemical ammonia synthesis: fundamental practices and recent developments in transition metal boride, carbide and nitride-class of catalysts. *Materials Advances*, *3*(13), 5207-5233. https://doi.org/10.1039/D2MA00279E

[29] Limmer, S. J., Chou, T. P., & Cao, G. (2003). Formation and optical properties of cylindrical gold nanoshells on silica and titania nanorods. *The Journal of Physical Chemistry B*, *107*(48), 13313-13318. https://doi.org/10.1117/12.451624

[30] Sun, C. (2018). On the plasmonic properties of Ag@ SiO2@ graphene core-shell nanostructures. *Plasmonics*, *13*(5), 1671-1680. https://doi.org/10.1007/s11468-017-0676-0

[31] Liu, L., Xu, X., Ye, Y., Ma, Y., Liu, Y., Lei, J., & Yin, N. (2012). Electrolysis synthetic silver nanoparticles enhanced light emission from CdSe quantum dots. *Thin Solid Films*, *526*, 127-132. https://doi.org/10.1016/j.tsf.2012.10.123

[32] Beyene, G., Sakata, G., Senbeta, T., & Mesfin, B. (2020). Effect of core size/shape on the plasmonic response of spherical ZnO@ Au core-shell nanostructures embedded in a passive host-matrices of MgF 2. *AIMS Materials Science*, *7*(6). https://doi.org/10.3934/matersci.2020.6.705

[33] Abbo, Y. A. (2021). Slow and fast lights in metal/dielectric composite of cylindrical nanoinclusions in passive and active linear dielectric host matrices. *Ukrainian journal of physics*, *66*(4), 281-281. https://doi.org/10.15407/ujpe66.4.281

[34] Hau, L. V., Harris, S. E., Dutton, Z., & Behroozi, C. H. (1999). Light speed reduction to 17 metres per second in an ultracold atomic gas. *Nature*, *397*(6720), 594-598. https://doi.org/10.1038/17561

[35] Getachew, S. (2024). Effect of Tunable Dielectric Core on Optical Bistability in Cylindrical Core–Shell Nanocomposites. *Advances in Condensed Matter Physics*, *2024*(1), 9911970. https://doi.org/10.1155/2024/9911970

[36] Getachew, S., & Shewam, S. (2023). LOCAL FIELD ENHANCEMENT OF CYL COMPOSITES IN PASSIVE A. https://doi.org/10.24941/ijcr.45824.11.2023

[37] Maier, S. A., & Maier, S. A. (2007). Surface plasmon polaritons at metal/insulator interfaces. *Plasmonics: Fundamentals and Applications*, 21-37. https://doi.org/10.1007/0-387-37825-1

[38] Pelton, M., & Bryant, G. W. (2013). *Introduction to metal-nanoparticle plasmonics*. John Wiley & Sons. https://doi.org/10.1080/00107514.2014.948921

[39] Prodan, E., Radloff, C., Halas, N. J., & Nordlander, P. (2003). A hybridization model for the plasmon response of complex nanostructures. *Science*, *302*(5644), 419-422. https://doi.org/10.1126/science.1089171

[40] Farokhnezhad, M., Esmaeilzadeh, M., Nourian, M., Jalaeikhoo, H., Rajaeinejad, M., Iravani, S., & Majidzadeh-A, K. (2020). Silica-gold nanoshell@ graphene: a novel class of plasmonic nanoagents for photothermal cancer therapy. *Journal of Physics D: Applied Physics*, *53*(40), 405401. https://doi.org/10.1088/1361-6463/ab95bf

[41] Shewamare, S., & Mal'nev, V. N. (2012). Two optical bistability domains in composites of metal nanoparticles with nonlinear dielectric core. *Physica B: Condensed Matter*, *407*(24), 4837-4842. https://doi.org/10.1016/j.physb.2012.08.007

Biography

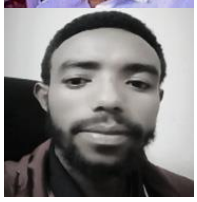

Tsegaye Atnaf is a Chemistry Lecturer at Wolkite University. He earned his Bachelor of Science degree in Applied Chemistry from Dilla University is 2017–2019, followed by a Master of Science in Organic chemistry in 2023. In his professional role, Tsegaye is responsible for teaching undergraduate courses and conducting research in natural product. He has extensive experience in reviewing and editing academic papers, particularly focusing on natural product.

Shewa Getachew is a Physics Lecturer at Wolkite University. He earned his Bachelor of Science degree in Applied Physics from Wolkite University is 2017–2019, followed by a Master of Science in Condensed Matter Physics in 2023. In his professional role, Shewa is responsible for teaching undergraduate courses and conducting research in material science. He has extensive experience in reviewing and editing academic papers, particularly focusing on optical properties and nanocomposites. His research interests span astronomy, space science, and material science, with a specific emphasis on the optical properties of nanocomposites, local field enhancement, and depolarization effects. Shewa's contributions have earned him notable recognition, including an award from the Ethiopian Physics Society in North America in 2022 and the SHEN Research Award in 2024. He is proficient in various technical tools such as Mathematica, MATLAB, Python, Fortran, and LaTeX, with expertise in scientific computing, optical simulations, and material science research.

Research Fields

Tsegaye Atnaf: Refractive index, group velocity of spherical Nanocomposites; Optical properties of core-shell nanocomposite of nanoparticles

Shewa Getachew: Local field enhancement of cylinderical Nanocomposites; Optical bistability of cylinderical Nanocomposites; Local field enhancement of spherical Nanocomposites; Optical bistability of spherical Nanocomposites; Refractive index, group velocity of spherical Nanocomposites